Time-resolved optical response of all-oxide $YBa_2Cu_3O_7/La_{0.7}Sr_{0.3}MnO_3$ proximitized bilayers

L. Parlato,[1] R. Arpaia,[1] C. De Lisio,[1] F. Miletto Granozio,[1] G. P. Pepe,[1] P. Perna,[2] V. Pagliarulo,[1] C. Bonavolontà,[1] M. Radovic,[3] Y. Wang,[4] Roman Sobolewski,[5,*] and U. Scotti di Uccio[1]

[1]*CNR-SPIN and Dipartimento di Scienze Fisiche, Complesso Universitario di Monte Sant'Angelo, Via Cinthia, I-80125 Napoli, Italy*

[2]*IMDEA-Nanociencia, Campus Universidad Autonóma de Madrid, 28049 Madrid, Spain*

[3]*Swiss Light Source, Paul Scherrer Institute, CH-5232 Villigen PSI, Switzerland and Laboratory for Synchrotron and Neutron Spectroscopy, EPFL, Lausanne, Switzerland*

[4]*Materials Science Graduate Program and Laboratory for Laser Energetics, University of Rochester, Rochester, New York 14627-0231, USA*

[5]*Institute of Electron Technology, PL-02668 Warszawa, Poland and the University of Rochester, Rochester, New York 14627-0231, USA*

(Received 12 April 2012; revised manuscript received 1 April 2013; published 22 April 2013)

We present femtosecond pump–probe spectroscopy studies of time-resolved optical reflectivity of all-oxide $YBa_2Cu_3O_7/La_{0.7}Sr_{0.3}MnO_3$ (YBCO/LSMO) superconductor/ferromagnet (S/F) bilayers consisting of a 100-nm-thick YBCO base layer and either 10 or 35 nm LSMO cap thickness. At temperatures far below the YBCO superconducting transition T_C, samples with a 10 nm F overlayer show a photoresponse that is similar to, but faster than, pure-YBCO, 100-nm-thick reference samples, while close to T_C and above (up to ∼160 K) we observe a signature of both the electronic and spin response that cannot be interpreted as an incoherent sum of contributions from the two layers. The photoresponse of the S/F structures with the 35-nm LSMO layer always qualitatively follows that of the pure LSMO, but with a shorter relaxation time. In all cases, the YBCO/LSMO nonequilibrium dynamics can be modeled using a generalized multitemperature model, which is a superposition of the dynamics of the three-temperature models that are used to describe the superconductor and ferromagnet subsystems, respectively. The long term of the photoresponse signal of the S/F bilayer can be well fitted with the two characteristic relaxation times.

DOI: 10.1103/PhysRevB.87.134514 PACS number(s): 74.40.Gh, 74.25.N−, 74.25.Gz

I. INTRODUCTION

The interplay between superconductivity (S) and ferromagnetism (F) is one of the most intriguing and challenging fields of research in condensed matter physics. The proximity effect at the interface between traditional conventional metallic S and F films has been widely investigated.[1] In comparison, properties of bilayers consisting of high-temperature superconducting cuprates and ferromagnetic manganites are much less understood, despite extended research activity and substantial progress in the comprehension of the physics of the involved materials.[2–4] The superconducting proximity effect at the S/F interface is governed by the short coherence length of the cuprate $\xi_0 = hv_F/2\Delta$ and by the even-shorter coherence length $\xi_m = hv'_F/E_{\rm exc}$ of manganites, where v_F and v'_F are the Fermi velocities in the S and F layers, respectively, Δ is the superconducting energy gap, and $E_{\rm exc} \approx 4$ eV is the manganite exchange energy.[5] As a consequence, ξ_0 and ξ_m are expected to be about 2 and 0.2 nm for $YBa_2Cu_3O_7$ (YBCO) and $La_{0.7}Sr_{0.3}MnO_3$ (LSMO), respectively. At the interface, a layer with a thickness of about ξ_0 within the superconductor is expected to show a depressed superconductivity that, in combination with extremely short ξ_m, suggests that Cooper pairs practically should not penetrate into the F layer. This simple consideration is a subject of a current debate since an unexpected, long-range-proximity effect has been recently reported[3,6,7] and ascribed to the spin superconducting triplet pairing at the F side of the bilayer in the presence of magnetic inhomogeneities or domain walls.[6,8]

Magnetic properties of the S/F interface, on the other hand, are governed by the short-length exchange field and associated with unconventional ordering of Cu spins,[4] while longer-range effects depend on the spin diffusion mechanism.[9] Finally, the establishment of the equilibrium chemical potential determines the charge transfer[2] with a screening length of the order of 1 to 2 nm, and it involves layers with depressed superconducting and magnetic properties ("dead layers") on both the S and F sides, respectively.

Cuprate/manganite-oxide nanostructured bilayers are likely to have a high potential for applications. Besides a constantly growing field of spintronics, our research attention has been devoted to YBCO/LSMO hybrids as possible artificially engineered, ultrafast optoelectronics devices.[10,11] The nonequilibrium properties of the S/F bilayers are far from being fully characterized and understood. However, some basic mechanisms are clear: When impinging photons deliver energy to the system, the electrons are promptly excited; then, an energy cascade follows, with the effect of redistributing the excess energy between electrons and phonons. The details are linked to specific material properties that are very different for a superconductor and a ferromagnet; but furthermore, some specific role of the interface might be envisaged. In this context, time-resolved femtosecond optical pump–probe spectroscopy is a unique investigation tool, extensively implemented in characterization of nonequilibrium carrier dynamics in various condensed-matter systems, ranging from metals and semiconductors to correlated-electron materials.[12,13] The system under study is perturbed by an ultrashort (femtosecond in duration) laser pulse (pump beam) and, next, this pump-induced reflectivity change is probed by a second, time-delayed femtosecond pulse. The very small variations in the reflectivity change of the probe beam are integrated and carry information on the nonequilibrium state dynamics of our system. The main advantage of this technique is its capability to follow, in time domain, the nonequilibrium

dynamics of relaxation on the time scale of the relevant phenomena, i.e., in the range 0.1 to 100 ps. In order to eliminate pump-to-probe jitter, both beams are optically split from the light generated by a single mode-locked femtosecond laser.

In this paper we present fabrication of epitaxial YBCO/LSMO nanobilayers along with their pump–probe characterization in a temperature range below and above the YBCO superconducting critical temperature T_C. The paper is organized as follows: In Sec. II the nonequilibrium photoresponse is described by first generalizing the standard two-temperature model for both the pure YBCO and LSMO samples and, next, combining it for the case of a bilayer S/F sample. An estimation of the relaxation times is obtained. In Sec. III we present a description of the samples fabrication and the experimental setup. The results of pump–probe measurements are presented in Sec. IV and discussed in terms of the earlier developed multitemperature model, and the characteristic relaxation times are extracted. A special emphasis is put on the role of the YBCO/LSMO interface. Finally, Sec. V summarizes our experimental and simulation results.

II. NONEQUILIBRIUM PHOTORESPONSE

When a laser pulse is absorbed by a metallic film, the electrons are abruptly driven out of the equilibrium. Within a few femtoseconds, the electron–electron (e–e) scattering causes the electron population to thermalize at a temperature T_e much higher than the sample temperature T_0. Subsequently, the excited electrons transfer their excess energy to the lattice optic and/or acoustic phonons via the electron–phonon (e–ph) interaction with a relaxation time $\tau_{e\text{–}ph}$ of the order of 1 to 10 ps, determining the increase of the phonon temperature T_{ph}. Finally, phonons cool down by either anharmonic decay or a direct heat transfer from the film to the substrate with a phonon escape time τ_{esc}. The time evolution of the above relaxation process can be described as the evolution of T_e and T_{ph} versus time, within the framework of the well-known two-temperature (2-T) model:

$$\begin{aligned} C_e \frac{dT_e}{dt} &= -g_{e\text{–}ph}(T_e - T_{ph}) + I(t), \\ C_{ph} \frac{dT_{ph}}{dt} &= -g_{e\text{–}ph}(T_{ph} - T_e) - \frac{C_{ph}}{\tau_{esc}}(T_{ph} - T_0), \end{aligned} \tag{1}$$

where $I(t)$ is the power released by the laser source in the unit volume and in our experimental case has a Gaussian shape with the full width at half maximum equal to 100 fs, C_e (C_{ph}) is the specific heat of electrons (phonons) and $g_{e\text{–}ph}$ is the effective e–ph coupling constant. The system has one fast, electronic relaxation time constant, given by $\tau_{e\text{–}ph} = (1/g_{e\text{–}ph})[C_e C_{ph}/(C_e + C_{ph})]$ and the thermal sink τ_{esc}. Note that in the final state, as described by this model, electrons and phonons share the same quasiequilibrium temperature, increased above the thermal bath T_0 by the amount $\Delta T^* = F/[d(C_e = C_{ph})]$, where $F = d\int_0^\infty I(t)dt$ is the fluence of the laser pulse and d is the thickness of the layer. The excess heat is transferred through the film and into the substrate due to acoustic phonons that propagate and cross the interface between film and substrate.[12,13] Thus, the heat diffusion dynamics is determined by extrinsic factors, i.e., it depends not only on the electronic properties of the excited material, but also on its ambient temperature, thermal coupling to the environment (substrate), as well as the pump-beam intensity. As a result, on a picosecond time scale typical for pump–probe experiments, the post-peak part of a transient photoresponse signal, especially collected under high pump intensity, often exhibits a nonzero plateau since the characteristic τ_{esc} is typically on the order of nanoseconds, i.e., is much longer than the measurement window. In most femtosecond pump–probe measurements, τ_{esc} has no influence on the observed nonequilibrium/electronic part of the sample reflectivity, as long as it is shorter than the laser repetition time.

In the case of "classical" (e.g., metallic) superconducting materials, the onset of superconductivity below T_C significantly changes the photoresponse dynamics. In this case, the laser pulse initially breaks Cooper pairs, thereby creating highly excited quasiparticles, which, as in the case of normal metals, thermalize through the e–e process almost instantaneously at a temperature T_e and relax toward the Fermi energy through an interaction with the phonon system, at a rate $\tau_{e\text{–}ph}^{-1}$. However, because of the superconducting 2Δ in their excitation spectrum, at the end of this energy cascade, quasiparticles pile up at the gap edge since they must recombine into Cooper pairs with the secondary acoustic phonon emission. This is a two-body process and under low excitation it is slow since the recombination rate τ_R^{-1} is proportional to the number of thermal quasiparticles available for recombination. In addition, simultaneous to the quasiparticle recombination process, already formed Cooper pairs can be broken again by the absorption of the earlier emitted recombination phonons.

In general, the nonequilibrium quasiparticle recombination process in superconductors is nonlinear and can be properly derived from the kinetic Eliashberg equations.[14] Subsequently, relaxation of photoexited quasiparticles is, in general, biexponential in character, implying two time constants, i.e., a fast time scale $\tau_{e\text{–}ph}$ and a slow time scale τ_R. Both $\tau_{e\text{–}ph}$ and τ_R depend on temperature and show a peak at $T \approx T_C$, due to the divergence of C_e. There are, however, different, simplified formulations leading to a single-exponential relaxation, and the most commonly used one is a so-called phenomenological Rothwarf and Taylor model,[15] which describes the time evolution of both the excited quasiparticle and phonon concentrations. The standard 2-T model has also been used quite successfully,[16,17] especially in the case of metallic (low-T_C) superconductors under relatively low perturbations. In the above case, $\tau_{e\text{–}ph}$ is close to τ_R and a single-exponential fit works well. In any case, as we mentioned earlier, τ_R^{-1} is proportional to the total number of quasiparticles, which in turn is an exponentially decreasing function of temperature.

In high-T_C oxide materials, the nonequilibrium relaxation dynamics is typically more complex as compared to metallic superconductors since recombination of two quasiparticles into a Cooper pair by emission of an acoustic phonon is in fact forbidden because the quasiparticle's velocity is larger than the sound velocity[18] and the Cooper-pair recombination reflects a complex kinematics involving both nodal and antinodal quasiparticles.[19,20] In order to fully account for both the fast thermalization of nodal quasiparticles and the slow process of the antinodal ones, we need to generalize the 2-T model

by writing separate rate equations for both types of relaxation channels. The resulting set of equations can written as

$$\begin{aligned} C_{Se}\frac{dT_{Se}}{dt} &= I_S(t) - g_{Se-ph}(T_{Se} - T_{Sph}) - g_{rec}(T_{Se} - T_{rec}),\\ C_{Sph}\frac{dT_{Sph}}{dt} &= g_{Se-ph}(T_{Se} - T_{Sph}) - g_{Sesc}(T_{Sph} - T_{S0}),\\ C_{rec}\frac{dT_{rec}}{dt} &= g_{rec}(T_{Se} - T_{rec}) - g_{Sesc}(T_{rec} - T_{S0}), \end{aligned} \quad (2)$$

where $I_S(t)$ is the optical pump $I(t)$, T_{Se} and T_{Sph} are the effective temperatures of optically excited electrons and the initial very fast optic phonons (nodal quasiparticle relaxation), followed by the thermalization process in the superconducting film, respectively. C_{Se} and C_{Sph} are the heat capacities of the two systems and g_{Se-ph} is the e–ph interaction constant, T_{rec}, on the other hand, represents the BCS-like relaxation, when antinodal quasiparticles recombine to form Cooper pairs via emission of acoustic phonons. C_{rec} is the heat capacity of the phonons, and $g_{rec} = \tau_R^{-1}$ is the recombination rate. T_{S0}, as before, is the thermal sink temperature, and $g_{Sesc} = C_{ph}/\tau_{esc}$ is phonon-escape constant, respectively.

Ferromagnetic materials, as superconductors, are characterized by a long-range order, but in this case the exchange field is due to the oscillations of the aligned spins, i.e., spin waves. In principle, spin waves can be excited by interactions with both electrons and phonons.[21,22] The corresponding rate equations, describing the system dynamics, are again similar to Eq. (1), but for the F films they include the temperature of spin waves T_s and, following Ref. 22, the resulting 3-T model can be written as

$$\begin{aligned} C_{Fe}\frac{dT_{Fe}}{dt} &= I_F(t) - g_{Fe-ph}(T_{Fe} - T_{Fph}) - g_{Fe-s}(T_{Fe} - T_s),\\ C_{Fph}\frac{dT_{Fph}}{dt} &= g_{Fe-ph}(T_{Fe} - T_{Fph}) - g_{Fph-s}(T_{Fph} - T_s)\\ &\quad - g_{Fesc}(T_{Fph} - T_{F0}),\\ C_s\frac{dT_s}{dt} &= g_{Fph-s}(T_{Fph} - T_s) + g_{Fe-s}(T_{Fe} - T_s), \end{aligned} \quad (3)$$

where $I_F(t)$ is the optical pump $I(t)$ and T_{F0} corresponds to T_0. C_s is the specific heat of spins, g_{Fe-s} and g_{Fph-s} are the electron-spin and phonon-spin coupling constants. It is generally assumed that in manganites the g_{Fe-s} interaction is of minor importance.[22] Therefore, the system is governed by the two time constants that describe the relaxation process of the e–ph and phonon-spin waves subsystems, respectively. The former (i.e., τ_{Fe-ph}) determines the fast component of the photoresponse relaxation dynamics; while the latter, defined as $\tau_{Fph-s} = (1/g_{Fph-s})[C_s C_{Fph}/(C_s + C_{Fph})]$, corresponds to the slow component. Above the Curie temperature, the slow dynamics disappears since the spin lattice loses its long-range order.

Let us now consider a bilayer formed by an F film "1" with the thickness d_1 and an oxide S film "2" with the thickness d_2. The following set of equations, which is a simple superposition of Eqs. (2) and (3) should hold:

$$\begin{aligned} C_{Fe}\frac{dT_{Fe}}{dt} &= I_F(t) - g_{Fe-ph}(T_{Fe} - T_{Fph}) - g_{Fe-s}(T_{Fe} - T_s)\\ &\quad - \frac{S_e}{d_1}(T_{Fe} - T_{Se}),\\ C_{Fph}\frac{dT_{Fph}}{dt} &= g_{Fe-ph}(T_{Fe} - T_{Fph}) - g_{Fph-s}(T_{Fph} - T_s)\\ &\quad - g_{Fesc}(T_{Fph} - T_{F0}) - \frac{S_{ph}}{d_1}(T_{Fph} - T_{Sph}),\\ C_s\frac{dT_s}{dt} &= g_{Fph-s}(T_{Fph} - T_s) + g_{Fe-s}(T_{Fe} - T_s),\\ C_{Se}\frac{dT_{Se}}{dt} &= I_S(t) - g_{Se-ph}(T_{Se} - T_{Sph}) - g_{rec}(T_{Se} - T_{rec})\\ &\quad + \frac{S_e}{d_2}(T_{Fe} - T_{Se}),\\ C_{Sph}\frac{dT_{Sph}}{dt} &= g_{Se-ph}(T_{Se} - T_{Sph}) - g_{Sesc}(T_{Sph} - T_{S0})\\ &\quad + \frac{S_{ph}}{d_2}(T_{Fph} - T_{Sph}),\\ C_{rec}\frac{dT_{rec}}{dt} &= g_{rec}(T_{Se} - T_{rec}) - g_{Sesc}(T_{rec} - T_{S0})\\ &\quad + \frac{S_{ph}}{d_2}(T_{rec} - T_{Sph}), \end{aligned} \quad (4)$$

where S_e and S_{ph} are the thermal conductance terms that describe the heat transfer by means of electrons and phonons across the F/S interface, respectively. Figure 1 schematically illustrates interactions between the subsystems mathematically described by Eqs. (4) and the associated coupling constants. One can realize that due to a large number of free/fitting parameters in Eqs. (4), it is very difficult to visualize a direct, physical insight into all processes involved. The dynamics of the F/S system can be simplified, however, under some assumptions. First, we note that the e–e interaction is so efficient (femtosecond time scale) that all electrons in our F/S bilayer share the same effective temperature from the very beginning of the relaxation, i.e., $T_{Fe} \approx T_{Se} \approx T_e$. We can also neglect, as before, the acoustic phonon heat transfer across the interface since it takes place on a much longer time scale (τ_{esc}), as compared to the electronic heat transfer. Finally, we can even decide to ignore the time-resolved dynamic of the spin subsystem relaxation since it is typically evolving on a time scale [$\tau_{ph-s} \approx 30$ ps (Ref. 22)] that is comparable or

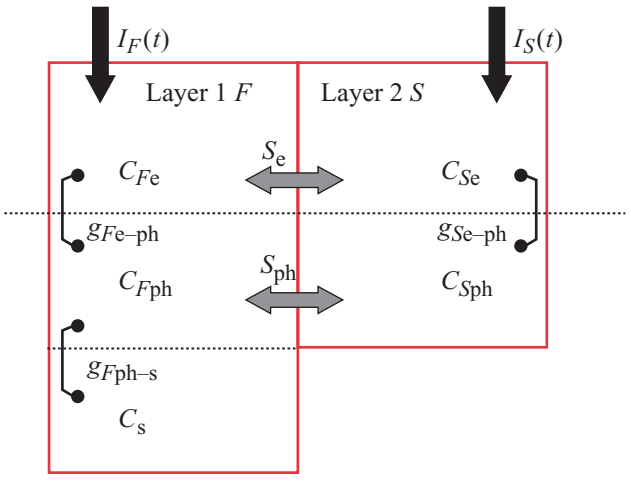

FIG. 1. (Color online) Schematics of the electronic and heat transfer in an S/F bilayer perturbed by an external optical excitation.

even longer than the standard observation time window in our experiments. Therefore, the spin system can be treated as a heat sink for an ultrathin F layer.

After some algebra, Eqs. (4) can reduce to the following set of four linear differential equations, combing the major dynamics effects:

$$\begin{aligned} C_{\mathrm{e}}\frac{dT_{\mathrm{e}}}{dt} &= I_F(t) - g_{F\mathrm{e-ph}}(T_{\mathrm{e}} - T_{F\mathrm{ph}}) + I_S(t) \\ &\quad - g_{S\mathrm{e-ph}}(T_{\mathrm{e}} - T_{S\mathrm{ph}}) - g_{\mathrm{rec}}(T_{\mathrm{e}} - T_{\mathrm{rec}}), \\ C_{F\mathrm{ph}}\frac{dT_{F\mathrm{ph}}}{dt} &= g_{F\mathrm{e-ph}}(T_{F\mathrm{e}} - T_{F\mathrm{ph}}) - g_{F\mathrm{esc}}(T_{F\mathrm{ph}} - T_{F0}), \\ C_{S\mathrm{ph}}\frac{dT_{S\mathrm{ph}}}{dt} &= g_{S\mathrm{e-ph}}(T_{\mathrm{e}} - T_{S\mathrm{ph}}) - g_{S\mathrm{esc}}(T_{S\mathrm{ph}} - T_{S0}), \\ C_{\mathrm{rec}}\frac{dT_{\mathrm{rec}}}{dt} &= g_{\mathrm{rec}}(T_{\mathrm{e}} - T_{\mathrm{rec}}) - g_{S\mathrm{esc}}(T_{\mathrm{rec}} - T_{S0}). \end{aligned} \quad (5)$$

The Eq. (5) set is applicable, of course, for the nonequilibrium relaxation dynamics of the bilayer when the F and S films are ferromagnetic and superconducting, respectively. For temperatures above T_C, the electron dynamics in the normal S film can be described by the standard 2-T model [Eq. (1)], and our multitemperature model for such bilayers is changed to

$$\begin{aligned} C_{\mathrm{e}}\frac{dT_{\mathrm{e}}}{dt} &= I_F(t) - g_{F\mathrm{e-ph}}(T_{\mathrm{e}} - T_{F\mathrm{ph}}) + I_S(t) \\ &\quad - g_{S\mathrm{e-ph}}(T_{\mathrm{e}} - T_{S\mathrm{ph}}), \\ C_{F\mathrm{ph}}\frac{dT_{F\mathrm{ph}}}{dt} &= g_{F\mathrm{e-ph}}(T_{\mathrm{e}} - T_{F\mathrm{ph}}) - g_{F\mathrm{esc}}(T_{F\mathrm{ph}} - T_{F0}), \\ C_{S\mathrm{ph}}\frac{dT_{S\mathrm{ph}}}{dt} &= g_{S\mathrm{e-ph}}(T_{\mathrm{e}} - T_{S\mathrm{ph}}) - g_{S\mathrm{esc}}(T_{S\mathrm{ph}} - T_{S0}). \end{aligned} \quad (6)$$

Equations (5) and (6) will be the starting point for our experimental data analysis presented in Sec. IV.

III. SAMPLES FABRICATION AND EXPERIMENTAL METHODS

YBCO/LSMO heterostructures were grown by pulsed laser deposition on (001) $SrTiO_3$ substrates (with a single TiO_2 termination layer) in an O_2 atmosphere at 0.25-mbar pressure for deposition of both the first (YBCO) and the second (LSMO) layers. The growth process was performed at 800 °C and controlled *in situ* by the reflection high-energy electron diffraction (RHEED) method. The RHEED patterns demonstrated very high crystallinity of our bilayer structures at every step of the process.[10] Cooling of the samples included a prolonged exposure to 200 mbar of O_2 at 500 °C to promote full oxidation of YBCO through the LSMO capping. The resulting nanostructures had excellent structural and transport properties, with ∼0.3° full width at half maximum rocking curves and the sharp superconducting transition (T_C up to 91.5 K, $\Delta T_C \sim 0.3$ K). Our test samples consisted of plain, 100-nm-thick YBCO and LSMO films, acting as reference samples, and a sequence of 100-nm-thick YBCO layers capped with a layer of LSMO, whose thickness ranged from 10 to 35 nm. By measuring the conductivity's dependence on temperature for a 100-nm-thick LSMO reference film, we deduced that its Curie temperature was above room temperature. Thus, in our experiments we expect that, especially at low temperatures, the 10 and 35-nm LSMO cap layers should remain in the ferromagnetic state even under optical illumination, although their Curie temperatures are likely to be reduced.

We stress that our LSMO/YBCO bilayers are optically active since the optical penetration depth δ for LSMO at the 800-nm wavelength is of the order of 200 nm, extrapolated from coherent acoustic phonon propagation measurements performed by Ren *et al.*,[23] while for YBCO $\delta \approx 66$ nm (Ref. 24). Thus in our experiments, the 10 and 35-nm LSMO cap layers are at least semitransparent, while YBCO is always optically active. To complete our studies (see Fig. 7), at one instance, we also grew an optically thick, 300-nm LSMO layer on top of a 100-nm-thick YBCO film.

The femtosecond pump–probe-spectroscopy experiments were performed using a mode-locked Ti:sapphire laser, which produced 100-fs pulses at 810-nm wavelength and a 76-MHz repetition rate. The pump and probe beams were focused onto the sample, down to 30 μm in diameter, and cross polarized to eliminate the coherent artifact caused by the direct interference of the two beams. The pump-to-probe average power ratio was set at least 10:1 with the probe power set at the 3-mW level (40 pJ of energy per pulse) to minimize probe-related optical heating and, simultaneously, ensure a good signal-to-noise ratio. The samples were mounted on a cold finger, inside a temperature-controlled, liquid-helium, continuous-flow optical cryostat, operating down to 4 K.

IV. REFLECTIVITY MEASUREMENTS AND DISCUSSION

Collecting our experimental data of the relative optical reflectivity change $\Delta R/R$ versus time delay we started with the pure, reference YBCO and LSMO films and the waveforms are presented in Fig. 2 (YBCO) and Fig. 3 (LSMO), respectively. In the case of YBCO, Fig. 2(a) presents the actual experimental $\Delta R/R$ waveforms obtained at different temperatures, while in Fig. 2(b) we compare selected traces recorded below T_C with the fits based on Eq. (2). We note that in agreement with earlier pump–probe studies performed on high-T_C materials under low-fluence excitations,[25,26] the amplitude of our $\Delta R/R$ signal [Fig. 2(a)] grows below T_C, while simultaneously the recovery becomes progressively slower. Overall our observations for the pure YBCO film are in agreement with the data reported for high-T_C materials[19,20,25–28] and corroborate the current interpretation that the slow dynamics below T_C (several tens of picoseconds) cannot be ascribed to the acoustic phonon bottleneck.[15] As shown in Fig. 2(b), the 3-T model developed by us for high-T_C superconductors [Eq. (2)] works very well and a biexponential relaxation is clearly visible near T_C, as is demonstrated in the inset in Fig. 2(b), where we show independently the nodal and antinodal relaxation dynamics.

In analogy to Fig. 2, Fig. 3(a) presents the experimental $\Delta R/R$ transients, this time collected for a pure LSMO film, while the corresponding fits, based on Eq. (3), are shown in Fig. 3(b). We note that the LSMO photoresponse is very different than that for YBCO. Within the shown temperature range the $\Delta R/R$ signal exhibits a negative, so-called photon bleaching effect, i.e., at the very early stage of relaxation, the pump-excited electrons remain in the excited state, so probe photons (note that pump and probe photons have the same energy in our pump–probe experiments) travel through

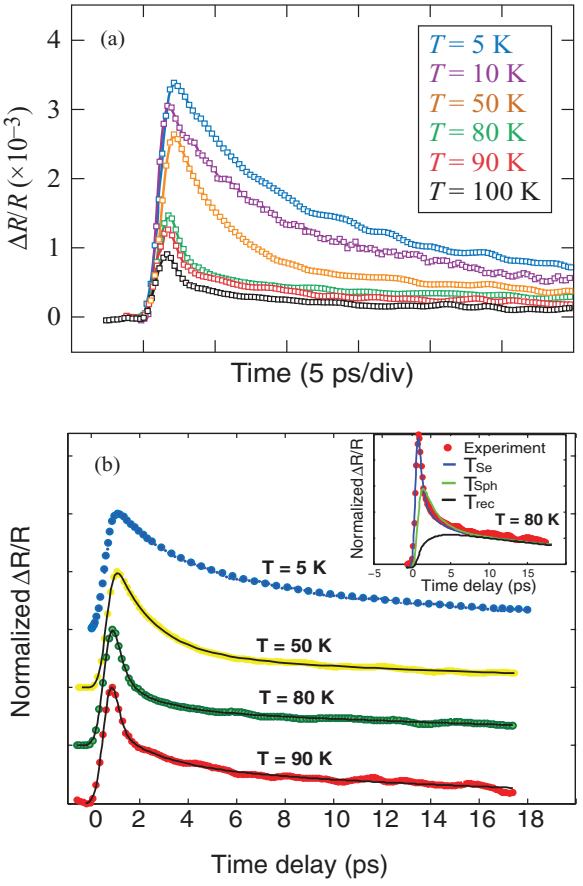

FIG. 2. (Color online) (a) The photoresponse $\Delta R/R$ transients versus time delay for a 100-nm-thick YBCO film measured at different temperatures within the 5 to 100 K range. (b) Selected traces from (a), normalized and fitted (solid lines) using a 3-T model listed in Eq. (2). The curves are shifted vertically for clarity. The inset in (b) shows the numerical fits corresponding to the nodal and antinodal YBCO relaxation dynamics [see Eq. (2)] at 80 K.

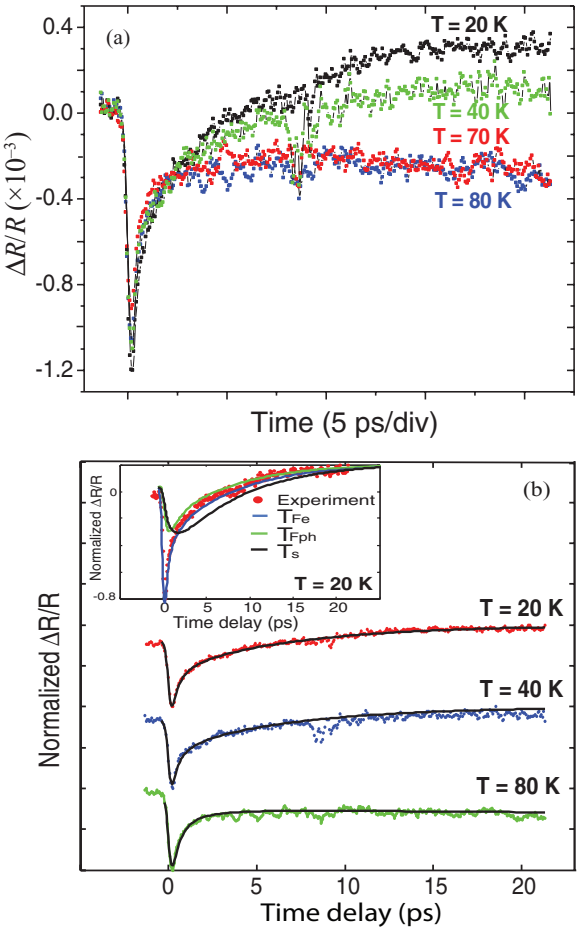

FIG. 3. (Color online) (a) The photoresponse $\Delta R/R$ transient versus time delay for a 100-nm-thick LSMO film measured at different temperatures within the 20 to 80 K range. (b) Selected traces from (a), normalized and fitted (solid lines) using a 3-T model listed in Eq. (3). The curves are shifted vertically for clarity. The inset in (b) shows the numerical fits corresponding to electron-spin and electron-phonon LSMO relaxation dynamics [see Eq. (3)] at 20 K.

the sample unabsorbed, resulting in transiently reduced reflectivity. Both the amplitude and the subpicosecond width of the initial bleaching transient remain roughly constant within the temperature range presented in the Fig. 3(a). The initial negative peak is followed by a double-exponential relaxation process, and a nanosecond-long, thermal diffusion plateau. The $\Delta R/R$ plateau was very sensitive to the intensity of the pump beam as well as temperature. For the fixed pump intensity of 3.2 μJ/cm^2 used to obtain the traces presented in Fig. 3(a), it switched from slightly negative (in the 60–90 K temperature range) to positive at the lowest, 20 K temperature, due to an apparent simple heating effect (slow dynamics of the heat diffusion process). The latter conclusion was corroborated by the observation that the increase of the pump intensity by the factor of 2 (to the 6.4 μJ/cm^2 value) resulted in the positive overshot of the plateau also in the 60–100 K range. Finally, at temperatures above 130 K the LSMO photoresponse signal started to rapidly decrease and in order to observe a measurable response (with decent signal-to-noise ratio) it was needed to significantly increase the pump intensity, but that immediately resulted in a heat-dominated signal with a large positive plateau component (not shown).

Overall our transient photoresponse for the pure LSMO film has been in agreement with general observations presented in Ref. 13 and the results described in Ref. 22. After the initial e–ph relaxation, we can identify a subsequent slower relaxation of the spin system. Figure 3(b) presents the same $\Delta R/R$ LSMO transients as in Fig. 3(a), but now they are normalized and overlaid with the fits based on the ferromagnetic 3-T model [Eq. (3)] with $I_F(t)$ negative to account for the bleaching effect. We note that, as in the case of the superconducting 3-T model for the pure YBCO film [see Fig. 2(b)], the ferromagnetic 3-T model (with the spin dynamics in an F film) describes very well the time-resolved nonequilibrium dynamics of the pure LSMO layer. The overall relaxation is about an order of magnitude slower, due to, as it was stressed in Ref. 22, a relatively slow spin dynamics. The effect is the most pronounced at the lowest temperatures, when the electron relaxation is even further slowed down by the heating effect, as we stressed before. The latter is clearly visible in the inset in Fig. 3(b), where we show independently the e–ph and the subsequent spin relaxation dynamics for the $\Delta R/R$ signal measured at 20 K. We note that both the $T_{F\,\mathrm{ph}}(t)$ and $T_s(t)$ components eventually

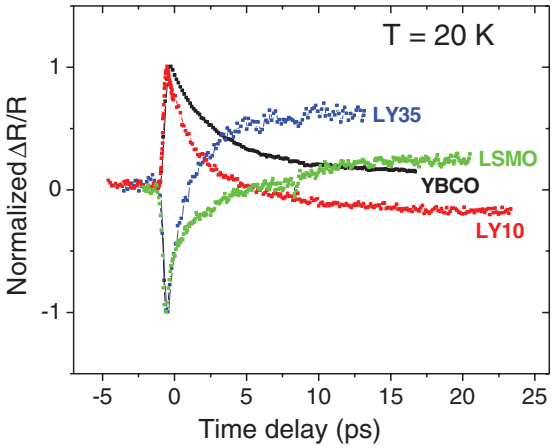

FIG. 4. (Color online) Normalized $\Delta R/R$ transients versus time delay measured at 20 K for our LY10 and LY35 bilayers, as well as the pure YBCO and LSMO reference samples.

drive the entire photoresponse signal into the positive values, supporting findings presented in Refs. 13 and 22 that, indeed, in thin LSMO films, the spin subsystem can be treated as a heat sink for nonequilibrium electrons.

Our next experimental step was photoresponse characterization of two YBCO/LSMO bilayers with a thickness of LSMO of 10 and 35 nm, respectively (named LY10 and LY35). Figure 4 presents an example of the data collected at 20 K (far below the YBCO T_C) for the LY10 and LY35 samples, as well as, for comparison, the pure YBCO and LSMO references. We observe that the thickness of the LSMO overlayer is of critical importance to the bilayer photoresponse. The temporal dependence of the LY10 $\Delta R/R$ waveform follows that of the YBCO sample, although with a shorter relaxation time. For the LY10 sample at low temperatures, the superconducting photoresponse clearly dominates and, as it will be shown later, it can be well simulated by the multitemperature model developed in Sec. II and given by Eq. (5). At the same time, the LY35 curve follows the LSMO $\Delta R/R$ transient, consisting of a initial bleaching peak, followed by a tail, which crosses into the positive values of the $\Delta R/R$ dependence. The initial relaxation of the LY35 $\Delta R/R$ transient is significantly faster than that of the pure LSMO layer, but the fast decay is followed by a very pronounced, positive lattice-heating plateau. Thus, the underlying YBCO film seems to only act as a heat sink.

Based on the observation presented in Fig. 4 and the fact that our research interest is focused on the superconducting properties of F/S bilayers, we have decided to restrict our further investigations to LY10 samples since in this case (as opposed to LY35) superconducting properties of the bilayer prevail, while, simultaneously, the influence of the F layer is non-negligible. A family of the $\Delta R/R$ photoresponse signals measured for LY10 at different temperatures is presented in Fig. 5, with the experimental waveforms (circles) collected: well below T_C, in the vicinity of T_C, and above T_C (with YBCO being normal). We note that as the experiment temperature is increased, even before we cross the T_C value, the waveforms change remarkably, and we observe a new oscillatory feature at the very early stages of the relaxation, pointing, as we will show later, to an active role of the F film and the

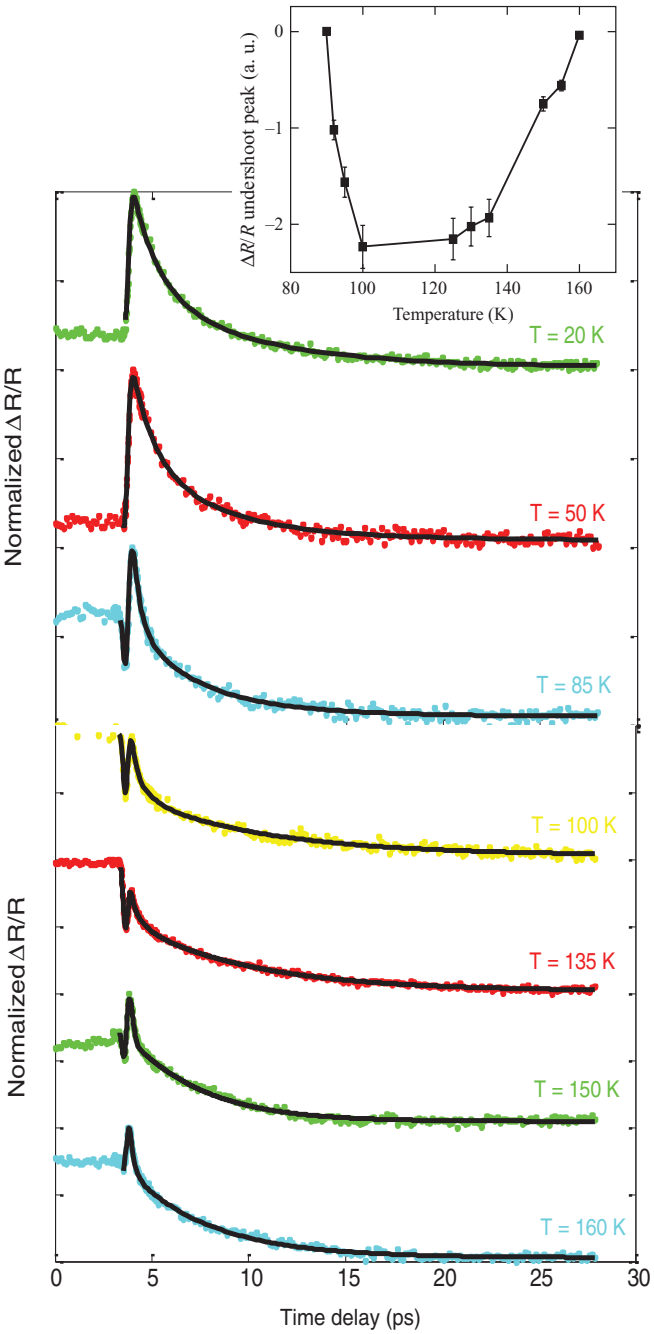

FIG. 5. (Color online) Normalized $\Delta R/R$ transients (dots) versus time delay for a LY10 sample at different temperatures below and above the YBCO T_C. The solid lines represent numerical fits based on Eq. (5) below T_C and Eq. (6) above T_C, respectively. The curves are shifted vertically for clarity. The inset shows the magnitude of the $\Delta R/R$ negative peak (undershot) versus temperature.

significance of the S/F interface. While at 50 K we still observe a "YBCO-like" positive transient [see Fig. 2], as temperature approaches T_C, a sharp and very fast undershot appears that precedes the positive $\Delta R/R$ peak. Most interestingly, as it is shown in the inset in Fig. 5, where we plot the amplitude of the $\Delta R/R$ peak undershot versus temperature, the undershot remains negative and roughly constant in the 100 to 140 K range, where YBCO is no longer superconducting, but LSMO

should still be magnetic. Finally, the negative component of the $\Delta R/R$ peak disappears completely at about 160 K, where, apparently, our 10-nm-thick LSMO layer, interfaced with a conducting oxide (YBCO above T_C), actually loses its magnetic ordering. Thus, above 160 K, we believe our entire bilayer can be just considered as a simple conducting oxide and fitted by the 2-T model. The pronounced negative plateau at high temperatures is due to the heating effect described before, namely, nanosecond in duration heat diffusion through the film and its transfer to the substrate.

We stress again that the behavior presented in Fig. 5 was highly reproducible, but it was observed only in the LY10 sample; the $\Delta R/R$ photoresponse of the LY35 at all tested temperatures was of the type shown in Fig. 4 and overall functionally followed the waveforms collected for the pure LSMO sample. As we have indicated in connection with Fig. 4, in the case of the LY35 sample, the thick LSMO layer simply dominates the dynamical response with YBCO acting as a heat sink.

The solid lines in Fig. 5 are the fits based on multitemperature rate equations listed in Eq. (5) for the traces collected below T_C, and in Eq. (6) for nonsuperconducting bilayers (above T_C). Although, due to a number of free-fitting parameters, we cannot draw any quantitative conclusions, our modeling gives excellent qualitative agreement and clearly indicates that the appearance of the undershot transient must be related to an additional, LSMO-related relaxation channel at the S/F bilayer. The most appealing possibility is a restricted charge transfer between the YBCO and LSMO layers with a possible influence of an ultrathin YBCO layer, "depressed," e.g., due to spins at the S/F interface. The excess electrons that are excited in YBCO reach the interface in a characteristic time $d/v_F \approx 100$ fs, comparable with our optical excitation pulse. However, their back injection into the LSMO layer is partially inhibited because a half-metal cannot host free electrons with both spin orientations. Reciprocally, the input of hot electrons from LSMO into YBCO is limited because they possess only one spin orientation. We stress that the above description is applicable both below and above T_C. Within the depressed YBCO below T_C, the quasiparticles experience a much faster recombination into Cooper pairs since this region acts as an energy trap (suppressed 2Δ region) that substantially shortens their relaxation process. On the other hand, above T_C the same depressed layer simply represents a source of extra traps resulting in the bleaching effect.

The concept of excitations being trapped at the boundary between a superconductor and a half-metal seems to be quite general, and the subject certainly deserves further investigation—both experimental and theoretical. From an experimental point of view, it is very suggestive to compare the observed dynamics of LY10 with that of underdoped oxide superconductors, such as oxygen-poor YBCO or $Bi_2Sr_2CaCu_2O_{8+y}$, both exhibiting a sharp, bleaching-type negative $\Delta R/R$ transient in a wide range of temperatures.[29–31] We intend to confirm the above observation in our future studies of LY10-type samples with the controllably depleted oxygen content in the YBCO film. Another interesting option is to study the quality of the LSMO/YBCO interface via propagation of coherent acoustic phonons, which can be generated and detected in femtosecond pump–probe experiments.[23,32]

During the course of our research, we have recorded dozens of $\Delta R/R$ waveforms for all LY10 samples measured in the temperature range from 4 to 300 K. As we have stressed before, our Eq. (5) set is too complex to give specific quantitative information, however, the post-peak relaxation dynamics clearly involves two characteristic relaxation rates:

$$\tau_f^{-1} = \frac{d_1 C_{Fe}\tau_{Fe-ph}^{-1} + d_2 C_{Se}\tau_{Se-ph}^{-1}}{d_1 C_{Fe} + d_2 C_{Se}}, \tag{7}$$

$$\tau_s^{-1} = \frac{d_1 C_{Fph} + d_2 C_{Sph}}{C_{Fph} + C_{Sph}} \frac{C_{Fe}\tau_{Fe-ph}^{-1} + C_{Se}\tau_{Se-ph}^{-1}}{d_1 C_{Fe}\tau_{Fe-ph}^{-1} + d_2 C_{Se}\tau_{Se-ph}^{-1}}. \tag{8}$$

The fast time τ_f is the effective relaxation time of electrons. It is an average of the e–ph interaction times in the two layers, with weights that account for the heat capacitance per unit area of each layer. The slow time τ_s is the time needed to reach the equilibration for both the F spin and S phonon subsystems and depends on the thickness ratio of the two slabs (see Fig. 1). The latter follows the intuitive idea that if one layer is much thicker than the other, it will dominate the relaxation dynamics. Following the above discussion, we can represent the nonequilibrium optical response of our S/F samples in terms of two phenomenological time constants, referred to as τ_{fast} and τ_{slow}, and write the experimentally measured normalized reflectivity change transient as

$$\frac{\Delta R}{R} = Ae^{-\frac{t}{\tau_{\text{fast}}}} + Be^{-\frac{t}{\tau_{\text{slow}}}} + C, \tag{9}$$

where the coefficients A and B are fitting parameters that describe the sample response to the optical excitation, while the constant C accounts for the background signal in the heat-diffusion final state. In general, A, B, and C can be either positive or negative, depending on the sample's properties and the experimental conditions, e.g., the pump intensity and/or substrate type.

The above coefficients are connected to the properties of the bilayer or, rather, its individual layers in a complex way. The amplitude reflection coefficient r of the bilayer can be given in terms of the amplitude reflection coefficients of both the overlayer r_1 and the bottom layer r_2 as

$$r = r_1 + \frac{\alpha(1 - r_1^2)r_2}{1 + \alpha r_1 r_2}, \tag{10}$$

where $\alpha = \exp(-2d_1/\delta)$ accounts for the optical absorption/transmission of the overlayer. It is clear that the bottom layer does not contribute to r when $r_1 \approx 1$ or when $\alpha \approx 0$ (i.e., the overlayer is thick enough to absorb all optical radiation before it reaches the bottom layer). In such a case it is expected that the coefficients A, B, and C are mainly related to the overlayer properties. For our F/S bilayers, the latter means that the $\Delta R/R$ photoresponse is dominated by the hot electron and spin relaxation dynamics of the F layer. On the other hand, if the overlayer is thin and $r_1 \ll 1$ the approximation $r \approx r_1 + r_2$ holds and A, B, and C will represent the average response of both materials. In the short time scale, the S contribution should prevail since the spin dynamics is relatively slow, as we have already indicated.

These considerations guide our phenomenological interpretation of the dynamic behavior of reflectivity versus time for the F/S bilayers: For F overlayers that are not too thick, the nonequilibrium state is shared by the two layers in a way that depends on the energy cascade, as illustrated

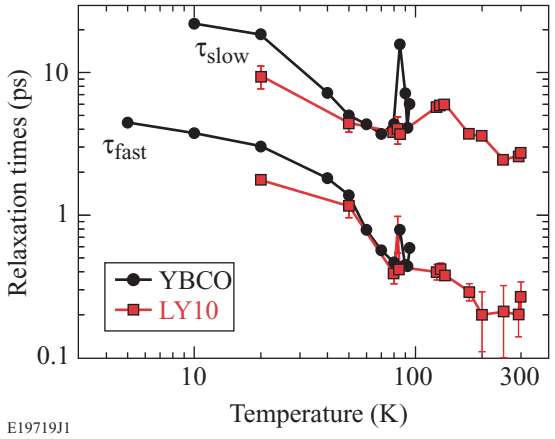

FIG. 6. (Color online) Characteristic fast and slow relaxation times (τ_{fast} and τ_{slow}) extracted from the experimental $\Delta R/R$ waveforms for our LY10 and pure YBCO samples as a function of temperature.

in Fig. 1. However, the pump-probe experiments sense the nonequilibrium state indirectly, i.e., through the variations of r_1, r_2, and α, and the time evolution governed by τ_{fast} and τ_{slow}.

We stressed that above T_C the fast time τ_{fast} was due to the e–ph interaction, while the slow time τ_{slow} was due to phonon equilibration. On the other hand, below T_C, the τ_{slow} must also be related to τ_R. Both τ_{fast} and τ_{slow} are expected to depend on the thickness of the F layers.

The results are summarized in Fig. 6, where we plot the τ_{fast} and τ_{slow} versus temperature for the LY10 and pure YBCO reference samples. First, we note a very pronounced, sharp peak near T_C for the YBCO τ_{slow} data, which we is due to the quasiparticle recombination time divergence and has been earlier reported in literature.[33] The same peak is missing in the LY10 trace, since, as we have demonstrated earlier (see, e.g., Fig. 5), in this temperature range the LY10 photoresponse

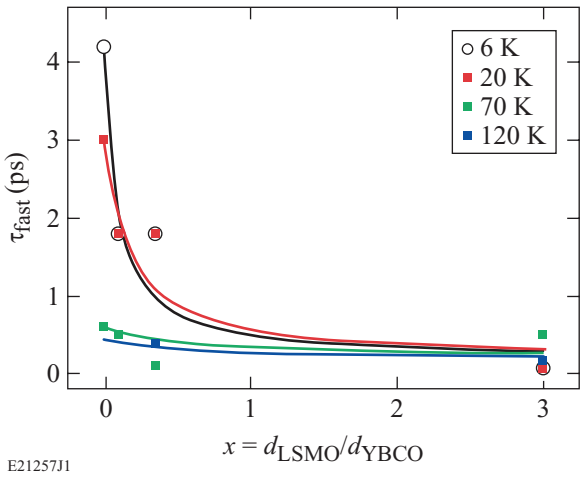

FIG. 7. (Color online) The fast characteristic relaxation time τ_{fast} versus the LSMO-to-YBCO thickness ratio collected for several F/S bilayers at different temperatures. The symbols refer to the experimental data at points $x = d_{\text{LSMO}}/d_{\text{YBCO}} = 0/100$, $10/100$, $35/100$, and $300/100$, respectively, while the solid lines are based on our theoretical model [Eq. (7)].

is strongly influenced by the dynamics of the F layer. The τ_{fast} values of the LY10 bilayer, especially far below T_C, are shorter than those of YBCO, resembling somewhat the behavior of YBCO/Au/NiCu multilayers.[10] Most interestingly and unexpectedly, contrary to the case of the metallic S/F proximitized bilayers,[17] we can actually identify the T_C peak features in τ_{fast} versus T dependences in both LY10 and YBCO. Finally, we stress that the measured values of τ_{fast} scale with the d_1/d_2 thickness ratio, in agreement with the general model described earlier in this section, as it is demonstrated in Fig. 7, where the solid-line fits correspond to Eq. (7).

V. CONCLUSION

We have investigated the nonequilibrium dynamics of YBCO/LSMO nanostructured bilayers in the temperature range from 4 K to room temperature. Using a generalized, multitemperature model, we have described a nonequilibrium relaxation dynamics of the electron subsystem in the both photoexcited YBCO and LSMO films and demonstrated that it could fit very well our experimentally measured, time-resolved $\Delta R/R$ photoresponse signals. Next we combined our modeling into a single set of linear differential equations in order to qualitatively represent the electron nonequilibrium dynamics in the LY10 sample both below and above the T_C value of the YBCO layer. Both the theoretical considerations, and the experimental time-domain $\Delta R/R$ results, unveiled a complex behavior that depended on both the thickness of bilayer materials and their interface. The most striking was a simultaneous presence of both the YBCO-like and LSMO-like, positive and negative, respectively, peaks in the very initial stage of the photoresponse at the temperatures between approximately 85 and 150 K.

Our experiments also demonstrated the existence of two main time scales in the post-peak exponential relaxation segment of the $\Delta R/R$ transients, of which the short one was evidently connected to the e–ph interaction. The fast time decay depended on the volume ratio between the bottom and top layers; this was consistent with the idea that the S/F system evolved from a photoexcited electronic state that equilibrated within itself in few tens of femtoseconds into a subsequent carrier relaxation processes that, in general, involved optic and acoustic e–ph scattering, in addition to the spin relaxation and quasiparticle recombination in the F and S layers, respectively. The longer time scale of the bilayer $\Delta R/R$ photoresponse was due to the quasiparticle recombination in YBCO and the phonon equilibration process, with the former dominating below T_C and the latter above T_C. Both time constants depended on temperature and showed a peak near T_C. The latter seems to be a signature of a superconducting state in the proximitized structure and is consistent with the long-range proximity effects, reported in literature for manganite/YBCO bilayer transport properties and arising from the magnetic inhomogeneity at the interface, where the magnetic exchange is compensated and the penetration of the order parameter is more favored.

The important and unique role of the LSMO/YBCO interface was observed in the photoresponse signals, collected for the LY10 sample in a wide temperature range across the superconducting transition. The $\Delta R/R$ transients measured

for S/F bilayers with a thick (35 nm) LSMO top layer were at all temperatures dominated by the LSMO photoresponse. Finally, the LSMO/YBCO bilayers with 10-nm-thick LSMO caps were characterized by quasiparticle relaxation times substantially shorter than those of the pure YBCO, making them interesting for possible applications in the field of ultrafast superconducting optoelectronics.

ACKNOWLEDGMENTS

The authors gratefully acknowledge D. Pan for assistance in some experiments. The work was partially supported by EU under the MAMA project (Napoli) and by the European Regional Development Fund through the Innovative Economy "MIME" grant POIG.01.01.02-00-108/09 (Warsaw). Additionally we acknowledge the EU COST Action MP1201.

*Corresponding author: roman.sobolewski@rochester.edu

[1] E. A. Demler, G. B. Arnold, and M. R. Beasley, Phys. Rev. B **55**, 15174 (1997).
[2] S. Yunoki, A. Moreo, E. Dagotto, S. Okamoto, S. S. Kancharla, and A. Fujimori, Phys. Rev. B **76**, 064532 (2007).
[3] V. Peña, Z. Sefrioui, D. Arias, C. Leon, J. Santamaria, M. Varela, S. J. Pennycook, and J. L. Martinez, Phys. Rev. B **69**, 224502 (2004).
[4] J. Chakhalian, J. W. Freeland, G. Srajer, J. Strempfer, G. Khaliullin, J. C. Cezar, T. Charlton, R. Dalgliesh, C. Bernhard, G. Cristian, H.-U. Habermeier, and B. Keimer, Nat. Phys. **2**, 244 (2006).
[5] J. Y. T. Wei, N.-C.Yeh, R. P. Vasquez, and A. Gupta, J. Appl. Phys. **83**, 7366 (1998).
[6] I. Asulin, O. Yuli, G. Koren, and O. Millo, Phys. Rev. B **74**, 092501 (2006).
[7] T. Holden, H.-U.Habermeier, G. Cristiani, A. Golnik, A. Boris, A. Pimenov, J. Humlícek, O. I. Lebedev, G. Van Tendeloo, B. Keimer, and C. Bernhard, Phys. Rev. B **69**, 064505 (2004).
[8] A. F. Volkov, F. S. Bergeret, and K. B. Efetov, Phys. Rev. Lett. **90**, 117006 (2003).
[9] S. Soltan, J. Albrecht, and H.-U. Habermeier, Phys. Rev. B **70**, 144517 (2004).
[10] G. P. Pepe, L. Parlato, N. Marrocco, V. Pagliarulo, G. Peluso, A. Barone, F. Tafuri, U. S. D. Uccio, F. Miletto, M. Radovic, D. Pan, and R. Sobolewski, Cryogenics **49**, 660 (2009).
[11] N. Marrocco, G. P. Pepe, A. Capretti, L. Parlato, V. Pagliarulo, G. Peluso, A. Barone, R. Cristiano, M. Ejrnaes, A. Casaburi, N. Kashiwazaki, T. Taino, H. Myoren, and R. Sobolewski, Appl. Phys. Lett. **97**, 092504 (2010).
[12] See, e.g., A. Othonos, J. Appl. Phys. **83**, 1789 (1998), and references therein.
[13] See, e.g., R. D. Averitt and A. J. Taylor, J. Phys.: Condens. Matter **14**, R1357 (2002), and references therein.
[14] G. M. Éliashberg, Sov. Phys. JETP **11**, 696 (1960).
[15] A. Rothwarf and B. N. Taylor, Phys. Rev. Lett. **19**, 27 (1967).
[16] M. Lindgren, M. Currie, C. A. Williams, T. Y. Hsiang, P. M. Fauchet, R. Sobolewski, S. H. Moffat, R. A. Hughes, J. S. Preston, and F. A. Hegmann, IEEE J. Sel. Top. Quantum Electron. **2**, 668 (1996).
[17] T. Taneda, G. P. Pepe, L. Parlato, A. A. Golubov, and R. Sobolewski, Phys. Rev. B **75**, 174507 (2007).
[18] B. J. Feenstra, J. Schützmann, D. van der Marel, R. Pérez Pinaya, and M. Decroux, Phys. Rev. Lett. **79**, 4890 (1997).
[19] P. C. Howell, A. Rosch, and P. J. Hirschfeld, Phys. Rev. Lett. **92**, 037003 (2004).
[20] C. W. Luo, L. Y. Chen, Y. H. Lee, K. H. Wu, J. Y. Juang, T. M. Uen, J.-Y. Lin, Y. S. Gou, and T. Kobayashi, J. Appl. Phys. **102**, 033909 (2007).
[21] E. Beaurepaire, J. C. Merle, A. Daunois, J. Y. Bigot, Phys. Rev. Lett. **76**, 4250 (1996).
[22] B. Mansart, D. Boschetto, A. Sambri, R. Malaquias, F. MilettoGranozio, U. Scotti di Uccio, P. Metcalf, and M. Marsi, J. Mod. Opt. **57**, 959 (2010).
[23] Y. H. Ren, M. Trigo, R. Merlin, V. Adyam, and Qi Li, Appl. Phys. Lett. **90**, 251918 (2007).
[24] L. Stojchevska, P. Kusar, T. Mertelj, V. V. Kabanov, Y. Toda, X. Yao, and D. Mihailovic, Phys. Rev. B **84**, 180507 (2011).
[25] M. L. Schneider, S. Rast, M. Onellion, J. Demsar, A. J. Taylor, Y. Glinka, N. H. Tolk, Y. H. Ren, G. Lüpke, A. X. Klimov, Y. R. Sobolewski, W. Si, X. H. Zeng, A. Soukiassian, X. X. Xi, M. Abrecht, D. Ariosa, D. Pavuna, A. Krapf, R. Manzke, J. O. Printz, M. S. Williamsen, K. E. Downum, P. Guptasarma, and I. Bozovic, Eur. Phys. J. B **36**, 327 (2003).
[26] N. Gedik, J. Orenstein, R. Liang, D. Bonn, and W. N. Hardy, Science **300**, 1410 (2003).
[27] X. Li, Y. Xu, Š. Chromik, V. Štrbík, P. Odier, D. D. Barros, and R. Sobolewski, IEEE Trans. Appl. Supercond. **15**, 622 (2005).
[28] X. Deng, M. Joshi, R. Chakalova, M. S. Colclough, R. Palai, Y. Y. Tse, I. P. Jones, H. Huhtinen, and C. M. Muirhead, Phys. Rev. B **77**, 144528 (2008).
[29] L. Shi, T. Gong, X. Weng, Y. Kostoulas, R. Sobolewski, and P. M. Fauchet, Appl. Phys. Lett. **64**, 1150 (1994).
[30] K. H. Wu, C. W. Luo, J. Y. Juang, T. M. Uen, and Y. S. Gou, Chin. J. Phys. **38**, 279 (2000).
[31] Y. H. Liu, Y. Toda, K. Shimatake, N. Momono, M. Oda, and M. Ido, Phys. Rev. Lett. **101**, 137003 (2008).
[32] I. Bozovic, M. Schneider, Y. Xu, R. Sobolewski, Y. H. Ren, G. Lüpke, J. Demsar, A. J. Taylor, and M. Onellion, Phys. Rev. B **69**, 132503 (2004).
[33] J. Demsar, B. Podobnik, V. V. Kabanov, T. Wolf, and D. Mihailovic, Phys. Rev. Lett. **82**, 4918 (1999).